Measurement Based Interference Models for Wireless Scheduling Algorithms

Helga Gudmundsdottir*§, Eyjólfur I. Ásgeirsson†‡, Marijke H. L. Bodlaender*‡, Joseph T. Foley†, Magnús M. Halldórsson*‡, Geir M. Järvelä*§, Henning Ulfarsson*‡ and Ymir Vigfusson*‡§

*School of Computer Science, ‡ICE-TCS, §CRESS
Reykjavik University, Iceland
E-mail: {helgag10,marijke12,mmh,geirmj11,henningu,ymir}@ru.is

†School of Science and Engineering
Reykjavik University, Iceland
E-mail: {eyjo,foley}@ru.is

***Abstract*—Modeling physical layer behavior of packet reception in the presence of interference is central to achieving efficient spectrum use in wireless sensor networks via spatial reuse. On one hand, analytic and simulations research has largely relied on assumptions of geometric path loss and isotropic transmission which have not been borne out in experiments. Experimental research, on the other hand, has not adopted theoretical models and instead focused on measuring the reality on the ground.**

We propose a new framework for wireless algorithms. First, distance-based path loss is replaced by an arbitrary gain matrix, typically obtained by measurements of received signal strength (RSS). This allows for the modeling of complex environments, e.g., with obstacles and walls. Second, a new parameter ζ indicates how close the gain matrix is to a distance metric, effectively measuring the complexity of the environment.

We experimentally validate our framework on two indoors testbeds with 20 and 60 motes. The results validate the basic properties of the model, the predictive ability of packet reception, dominance over distance-based models, and the sensitivity of ζ to the nature of the environment. Theoretically, we show that *all* known SINR scheduling algorithms that work in general metric spaces carry over and achieve equivalent performance guarantees in the new model. The conclusions suggest that wireless theory can finally be grounded in experimental practice.

I. Introduction

There is mounting demand for tomorrow's wireless networks to provide higher performance while lowering costs. A central challenge in meeting this demand is to improve the utilization of the wireless spectrum to accommodate simultaneous communications at the same radio frequency. To accommodate research seeking to provide efficient use of wireless channels at large-scale, for instance through spatial reuse, we require good models of the behavior of signal propagation and reception at the physical layer in the presence of wireless interference.

Early models of wireless communication under interference were graph-based, most commonly based on distances. In comparison, physical models, or *SINR* (signal to interference and noise ratio) models, capture two important features of reality: signal strength decays as it travels (rather than being binary) and interference accumulates (rather than being a pairwise relation).

Analytic work on SINR – introduced by Gupta and Kumar [17] in an average-case setting and Moscibroda and Wattenhofer [36] in worst-case – has almost entirely assumed *geometric path loss*, referred to here as the GEO-SINR model: signals decay as a fixed polynomial of the distance traveled. While this assumption is indeed correct in free space, *actual* environments involving wireless networks are more challenging.

When located above an empty plane, a signal bounces off the ground, resulting in complicated patterns of superpositions known as *multi-path fading*. Most real scenarios are more complex, with walls and obstructions. In particular, cityscape and indoor environments are notoriously hard to model.

Many experimental results have shown that not only are the simple range-based models naïve, but so are the geometric path loss assumptions of smooth and isotropic polynomial decrease in signal strength. In fact, quoting recent meta-analysis [3], "link quality is not correlated with distance."

As a result, experimental research has moved away from *prescriptive* models such as GEO-SINR towards *descriptive* models based on measurements [42]. The additivity assumption of the SINR model has been validated in several studies, permitting decisions to be based on measuring interferences from individual nodes rather than from arbitrarily-sized subsets simultaneously.

Wireless research is therefore experiencing a chasm between theory and practice. In particular, the lack of fidelity of its models leaves theoretical work in abeyance. Especially, the *raison d'être* for SINR research was after all supposed to be greater realism. On the other hand, allowing for *arbitrary* path loss results in computational problems with extremely strong approximation hardness results [14], [23]. This places algorithmic research in the quandary of choosing between intractability or lack of fidelity.

We are therefore led to a challenge:

> *Can we model wireless communication in a way that is faithful to reality, general enough to capture wide range of situations and technologies, yet amenable to algorithm design and analysis?*

Our contributions: (i) We propose to replace geometric path loss with a matrix representing the fading (or *gain*) between pairs of nodes. This matrix can capture arbitrary environmental settings, allowing for asymmetry, anisotropic transmissions, shadowing, and complex fading patterns. To avoid the computational intractability of an unconstrained "abstract SINR" setting, we introduce a measure that reflects

the attenuation complexity of the scenario. Dubbed *metricity* and denoted ζ, this parameter intuitively represents how close the gain matrix is to a distance metric. The gain matrix is typically generated from direct measurements of *received signal strength* (RSS) that motes provide, as proposed by experimentalists [44], [42], [34]. These measurements, however, could also be generated by other means, such as by inference, history, or by accurate environmental models. We refer to this measurement based model as MB-SINR.

(ii) We have verified the key features of our framework in experiments on two testbeds of 20 and 60 nodes. In particular, we show that the additivity holds, that estimated SINR is a good prediction of packet reception rate, and that the MB-SINR model significantly outperforms GEO-SINR. We also discover that temporal factors are not a concern in a static environment beyond the effects of external networks. Additionally, we find the metricity parameter to be moderate and that it properly reflects the complexity of the environment.

(iii) From the standpoint of theoretical analysis, the definition of MB-SINR has extensive implications: *SINR algorithms that work in arbitrary metric space, work equally well in* MB-SINR. *The performance ratio, in terms of ζ, is equivalent to the original algorithm's dependence on α.*

In particular, a raft of results holds without change for some of more fundamental scheduling problems of the MAC layer, like LINK CAPACITY (a.k.a., *maximum independent set of links*, or *single-shot scheduling*) and LINK SCHEDULING (a.k.a., *minimum length link scheduling*). As a "proof of concept", we illustrate the approach by generalizing the previous constant-approximation algorithm for LINK CAPACITY to a multiple-channel version in MB-SINR. We also use the opportunity to improve the dependence of the approximation factor on ζ (or α).

Roadmap: In the following section, we formally define our concepts. We present our experimental results in Section III and the theoretical results in Section IV. We survey related work in Section V and conclude in Section VI. An omitted proof is provided in the appendix.

II. PHYSICAL MODELS

The SINR model has two key properties: **(i)** signal decays as it travels from a sender to a receiver, and **(ii)** interference – signals from other than the intended transmitter – accumulates. Transmission succeeds if and only if the interference is below a given threshold.

Formally, a *link* $\ell_v = (s_v, r_v)$ is given by a pair of nodes, sender s_v and a receiver r_v. The channel *gain* G_{uv} denotes the decay in the signal of ℓ_u as received at r_v. If a set S of links transmits simultaneously, then the SINR at ℓ_v is

$$\text{SINR}_v := \frac{P_v G_{vv}}{N + \sum_{u \in S} P_v G_{uv}} \ , \tag{1}$$

where P_v is the power used by the sender s_v of ℓ_v, and N is the ambient noise. In the *thresholded* SINR model, the transmission of ℓ_v is *successful* iff $\text{SINR}_v \geq \beta$, where β is a hardware-dependent constant.

The standard analytic assumption of *geometric path loss* states that the gain is inversely proportional to a fixed polynomial of the distance traveled, *i.e.*, $G_{uv} = d(s_u, r_v)^{-\alpha}$, where the *path loss factor* α is a constant between 1 and 6. This assumption is valid in free space; we have $\alpha = 2$ in perfect vacuum.

Metricity: We assume arbitrary path loss, where $G_{uv} = 1/f(s_u, r_v)$ for some function f of pairs of points. We introduce a parameter ζ that represents how close the measured gains are to a distance metric. The *metricity* ζ of a given gain matrix is defined to be the smallest number satisfying for every triplet x, y, z,

$$f(x,y)^{1/\zeta} \leq f(x,z)^{1/\zeta} + f(z,y)^{1/\zeta} \ . \tag{2}$$

Note that ζ is well-defined, since $\zeta \leq \max_{x,y} \lg f(x,y)$. In the case of geometric path loss, $\zeta = \alpha$, since $f(x,y) = d(x,y)^\alpha$ and the distance function $d(x,y)$ satisfies the ordinary triangle inequality.

The MB-SINR model refers to the combination of the SINR formula applied to a general gain matrix G, typically obtained as RSS measurements, along with a metricity parameter ζ.

III. MODEL VALIDATION

We can now revisit the empirical portion of our initial research question, specifically of modeling wireless communication in a manner that is *faithful to reality* in a wide range of situations. Below, we assess the predictability of packet reception rate (PRR) under interference by comparing our MB-SINR model to the original GEO-SINR through experiments. Our experiments are conducted in two testbeds (Fig 2): one in the middle of a large open classroom (TB-20) and another in a challenging basement corridor (TB-60). Our results suggest that MB-SINR is a good predictor of PRR, and significantly better than using geometric path loss information alone. Finally, we measure and discuss values for the metricity parameter ζ in the different testbeds.

A. Experimental Setup

Wireless hardware: Since a motivating goal of our study is to understand raw interference between wireless transceivers, we elected to operate at the physical-layer of a wireless device. We needed a mote with granular control over MAC-level capabilities, such as power and frequency control, over one tailored to specific protocol stacks, such as the 802.11 suite. For example, we require the ability to disable low-level features such as clear channel assessment (CCA).

We chose the Pololu Wixel, a development board for the TI CC2511F32 [45], as our mote hardware platform. The CC2511F32 is an 8051 micro controller SystemOnChip with integrated 2.4 GHz FM-transceiver stage (CC2500). In addition to meeting our functional requirements, the Wixels are inexpensive (14–20 USD), enabling larger scale deployments.

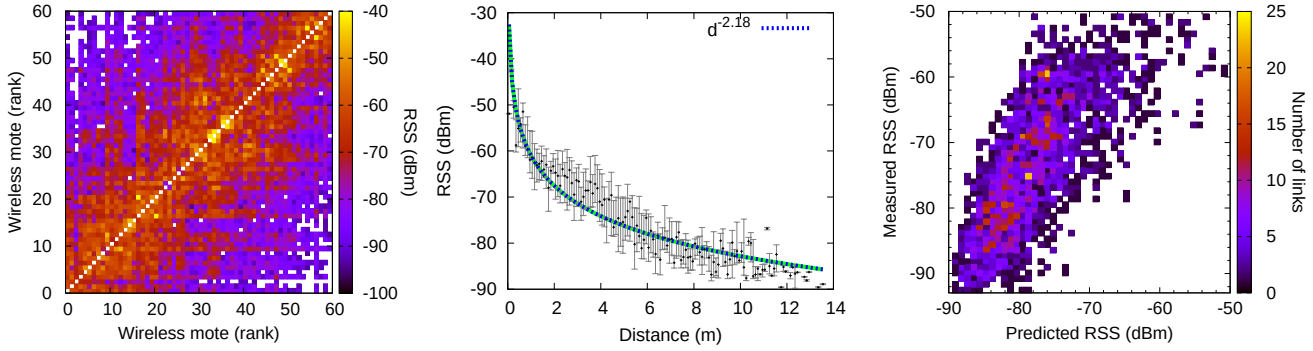

(a) RSS matrix. (b) Evaluating path loss constant. (c) Comparing RSS and geometric path loss ($d^{-\alpha}$).

Fig. 1: **(a) RSS matrix.** Gain between directed pairs of nodes in TB-60, measured by RSS and averaged over 1000 packets. **(b) Estimating the α path loss constant.** The median received signal strength (RSS) decreases with distance from the transmitter. The striped line shows the function $d^{-2.18}$, where the α-exponent was obtained via least-squares linear regression. **(c) Comparing measured and predicted RSS.** Correlation between RSS as predicted by distance with geometric path loss (x) and measured in TB-60 testbed (y).

Configuration: In our experiments, every sender node in each trial transmits a burst of 1000 packets with 4 ms delay between consecutive packets to facilitate successful delivery to the receiver. The length of each packet is 22 bytes, including a 16 bit CRC. Only packets that pass a CRC check are considered successful transmissions, with all error correction capabilities on the mote disabled. The radio is configured to use data whitening and Minimum Shift Keying (MSK) modulation format. During experiments, the wireless motes report details about packets sent or received to an auxiliary log via USB which also provides control signals and power for the experiments. Packet details include the received signal strength (RSS) as an integer in dBm.

Classroom testbed: In the first testbed (TB-20), we arranged 20 wireless motes on an 4×5 grid with 1 m spacing. The motes in the grid were mounted on wooden poles 1 m from the ground in order to minimize reflection and attenuation from the ground; see Fig. 2 for the topology. Due to the challenges of scheduling a sufficiently large classroom for an extended duration, this testbed was deployed temporarily for a focused set of tests.

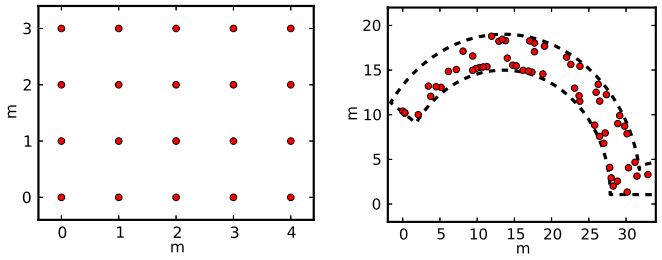

Fig. 2: Topologies of our 20-node testbed (TB-20) **(left)** and 60-node curved corridor testbed (TB-60) **(right)**.

Basement corridor testbed: In the second testbed (TB-60), we suspended 60 wireless motes about 0.3 m from metal wire trays and 2.5 m from the concrete floor in a curved basement corridor; see Fig. 2 for the topology. Due to the arced positioning, we used polar coordinates to locate the motes. The corridor provides a challenging environment: limited line of sight between motes, obstacles such as water pipes and thick electric cables, and reinforced concrete walls. Approximately 94% of the directed links are in range for communication. The length of the corridor is 40.1 m, the longest distance (direct line) between any two motes is 21.8 m while the shortest distance is 0.4 m. The TB-60 testbed is a more permanent setup, with the experiments conducted over the span of several weeks.

B. Model calibration

We ran several experiments on the testbeds to gather calibration data for both models. For figures with error bars, x-coordinate shows the median, and upper and lower quartiles of the distribution of trials.

Ambient noise parameter N: We evaluated N by sampling the noise level registered by each mote, over several hours in both early morning and during nighttime. We observed minimal external interference at 2.44 GHz. All of our experiments use that frequency unless otherwise stated. We found the average ambient noise in TB-60 to be around -99.1 dBm, but considerably higher in TB-20 at around -94.4 dBm, in part due to external interference from 802.11 infrastructure.

Power setting P: We configured the wireless mote's transmission power to 1 mW in all of our experiments, and normalize the P parameter as 1.

RSS matrix: We measured the RSS for all directed node pairs (s_v, r_v) in both testbeds. In each time slot, a chosen node transmits 1000 packets in a sequence, while other nodes

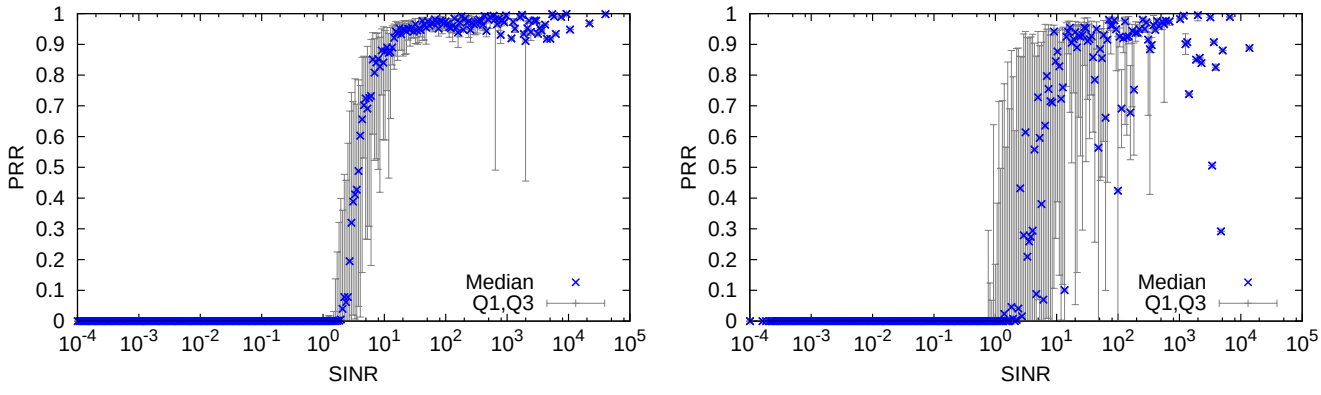

(a) MB-SINR (b) GEO-SINR

Fig. 3: **Packet reception rate for (a) MB-SINR (b) GEO-SINR.** Fraction of packets correctly decoded by receivers in TB-60 as the SINR is varied by evaluating different pairs while possibly invoking multiple senders. The plots show a phase transition between 0 to 100% PRR as the SINR grows.

act as receivers. The procedure was repeated for each pair of directed nodes. For temporal robustness, including day and night variations, the experiments were repeated at different times of the day.

Fig. 1a illustrates the RSS_{vv} for all node pairs (s_v, r_v) in testbed TB-60. The motes on both axes are ordered by the angle of their polar coordinates, making adjacent motes in Fig. 1a likely to be physically close in the testbed. The heatmap shows graphically that physical proximity correlates with high RSS between a pair of nodes.The figure also demonstrates that every mote can hear some other mote in the testbed, that some mote pairs cannot communicate, and that transmissions are not fully symmetric.

Path-loss constant α: The geometric SINR model captures the attenuation of a wireless signal from sender s_v to receiver r_v over distance by assuming the RSS is proportional to $d(s_v, r_v)^{-\alpha}$, where α is a path loss parameter. Fig. 1b shows the estimation of α. Given link lengths and the RSS values from Fig. 1a, the best linear least-squares fit is for $\alpha = 2.18 \pm 0.07$.

Fig. 1c shows the correlation between the predicted RSS and the measured RSS. The predicted RSS values are based on geometric path loss $d(s_v, r_v)^{-\alpha}$ with the fitted α-value of 2.18. If the prediction was perfect, we would see the points fall on the $y = x$ diagonal line. However, the points in Fig. 1c are very scattered and do not indicate that geometric path loss is a reliable predictor for RSS.

C. Comparing the GEO-SINR and MB-SINR models

We next evaluate the predictive power of the two models in experiments with varying interference.

Forcing wireless interference in practice: One of the challenges with hardware experiments is the synchronization of the wireless motes. Our focus on measuring interference requires us to ensure that interfering motes are transmitting at the same time as the sender. Although we investigate sets of links that are transmitting at the same time, our analysis is focused on the performance of individual links. We therefore circumvent the problem of synchronizing the motes by running our experiments for each individual link in the link set. To analyze how a single link ℓ_v would perform in the presence of the other sender-receiver pairs in a set S, we make the links in $S \setminus \{\ell_v\}$ transmit continuously while we measure the transmission of ℓ_v. The continuous transmission by other senders ensures that the receiver in link ℓ_v experiences interference from other links.

Experimental design: With the synchronization issues in mind, we devised an experiment to compare the predictive power of the two models. We repeatedly select a random pair of nodes to act as sender and receiver, and a subset of 1–10 other nodes to cause interference. During the trial, the interfering nodes continuously transmit packets on the same frequency. We deploy low-level packet filtering at the receiver to minimize processing overhead due to interfering packets.

Packet reception rate by model: A successful transmission of a packet depends on the signal strength of the transmission, ambient noise and the amount of interference from other nodes. The SINR model uses the ratio of the received signal over the sum of ambient noise and the cumulative signal strength of other senders. If this ratio is above some threshold the transmission is considered successful, otherwise it is assumed that the transmission has failed.

We generated over 15,000 trials and looked at the packet reception rate as a function of the SINR as calculated by the two models. Fig. 3a shows the PRR as a function of the SINR in MB-SINR, calculated using the RSS matrix shown in Fig. 1a. Corresponding results are shown in Fig. 3b, where the SINR is based on distances between nodes, as in GEO-SINR.

We can see that MB-SINR behaves as expected: generally the PRR and SINR values are either both small or both large. There is a swift transition where the PRR increases rapidly. We

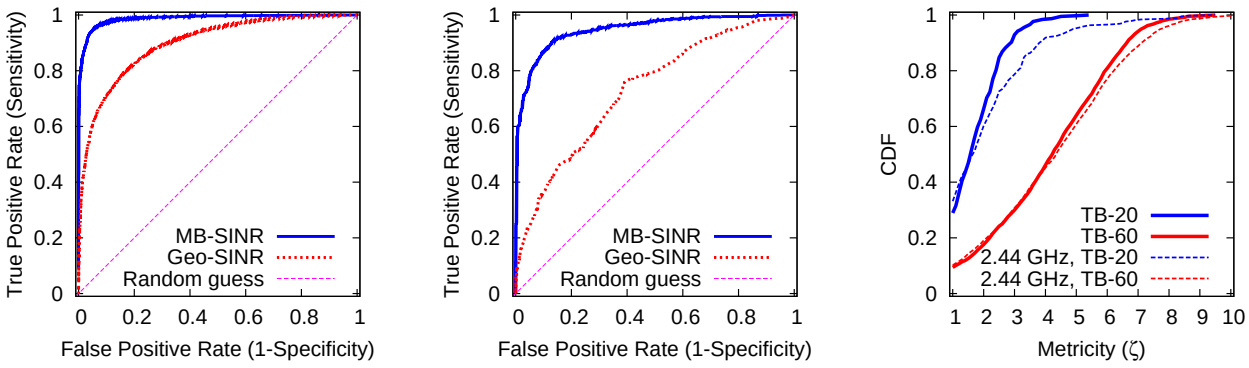

(a) ROC-curve for TB-60 (b) ROC-curve for TB-20 (c) Metricity (ζ) in TB-20 and TB-60

Fig. 4: **ROC-curves for (a) TB-60 and (b) TB-20.** Comparison of MB-SINR and GEO-SINR as estimators for successful transmission of packets as the acceptance threshold is varied. Each trial consists of 1000 packets exchanged in TB-60. A positive trial outcome has PRR $\geq 80\%$ whereas a negative one has PRR $\leq 20\%$. **(c) Metricity (ζ)** CDF comparison of computed ζ values for RSS matrices on both testbeds. The thick lines represent values computed for the $\widehat{\text{RSS}}$ matrices. The dashed lines show ζ values for the 2.44 GHz frequency, which is representative of other frequencies in the respective testbeds.

note that occasional trials produce a small PRR value despite SINR being large, as indicated by the two large error bars where SINR $\approx 10^3$. These outliers stem from occasionally no packets being received even for a large SINR, likely due to details originating in the testbed topology, such as destructive interference caused by signal reflection. Nevertheless, the MB-SINR model has a discernible threshold indicating whether or not a transmission is successful.

The GEO-SINR model does not show the same clear behavior in our experiments. The same general relationship between SINR and PRR manifests itself, but the model does not exhibit the same well-defined threshold as that of MB-SINR. In other words, the predictive power of the SINR appears to be significantly smaller for GEO-SINR than for MB-SINR. To analyze this behavior, we further evaluate the predictive accuracy of the two models.

Sensitivity and specificity analysis: The GEO-SINR and MB-SINR models can be viewed as binary classifiers that compare the SINR to a threshold (β) to determine whether a transmission will be successful or not. We say that a transmission is experimentally successful if PRR $\geq T_{high}$ and declare it a failure if PRR $\leq T_{low}$. We focus on those links that were clearly either feasible or infeasible in our experiments, and set $T_{high} = 0.8$ and $T_{low} = 0.2$. Roughly 6% of the tested links fall within the $0.2 - 0.8$ range and are thus not considered. A single instance in an SINR binary classifier can have four outcomes:

- True positive (TP): SINR $\geq \beta$, PRR $\geq T_{high}$
- False positive (FP): SINR $< \beta$, PRR $\geq T_{high}$
- True negative (TN): SINR $< \beta$, PRR $< T_{low}$
- False negative (FN): SINR $\geq \beta$, PRR $< T_{low}$

A binary classifier incurs an inherent trade-off between true positive rate (sensitivity), defined as $\frac{\text{TP}}{\text{TP+FN}}$, and false positive rate (1-specificity), defined as $1 - \frac{\text{TN}}{\text{FP+TN}} = \frac{\text{FP}}{\text{FP+TN}}$. The trade-off balance can normally be tuned by a threshold parameter of the classifier, in this case β. By varying β, the trade-off can be graphically depicted on a ROC-curve (Receiver Operating Characteristic) that shows true and false positive rates on two axes. If $\beta = 0$, the classifier predicts that all transmissions will be successful, and if β is large, the classifier predicts that all transmissions will fail. A naïve classifier making uniformly random guesses would fall on the diagonal line from $(0, 0)$ to $(1, 1)$, whereas the $(0, 1)$ point denotes perfect classification.

Fig. 4a and 4b show the ROC-curves for the TB-60 and TB-20 testbeds, respectively. MB-SINR provides significantly better classification than GEO-SINR. In TB-60, the best trade-off between true and false positive rates occurs when $\beta = 2.15$, with a true positive rate of 94.8% and false positive rate of 5.2%.

In contrast, the predictions made by the canonical GEO-SINR on the same testbed plateaus at true positive rates of 81.4% and false positive rates of 18.6%. Both models give less accurate predictions for TB-20 compared to TB-60. The topology for TB-20 is more compact than TB-60, with fewer number of trials. The larger and more variable ambient noise in TB-20 makes it more difficult to accurately predict the outcome of a transmission than in the TB-60 testbed.

Overall, MB-SINR provides significantly superior predictive power for PRR than GEO-SINR on both testbeds. Our results are robust against modifying the thresholds to $T_{high}, T_{low} = 0.5$. Note that RSS measurements used to compute SINR in MB-SINR were performed weeks in advance of these experiments. This suggest that the RSS matrix is resilient to temporal factors, with MB-SINR correctly predicting nearly 95% of all instances.

Additivity of interference: One of the assumptions made in the SINR model is that interference is additive. In other words, if multiple senders transmit simultaneously, we estimate the RSS at the receiver to be the sum of the individual signals.

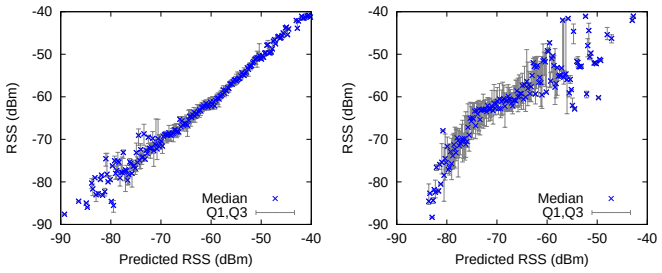

(a) Additivity in MB-SINR (b) Additivity in GEO-SINR

Fig. 5: **Additivity in (a) MB-SINR and (b) GEO-SINR** Correlation between predicted and measured (RSS) in TB-60.

Figs. 5a and 5b show the actual RSS as a function of the predicted RSS as given by MB-SINR (Fig. 5a) and GEO-SINR (Fig. 5b). We note that the variability evident in the measured RSS arises due to sparsity of data in those regions. If the additivity assumption is true, we would expect the values in the figures to fall on the diagonal line $y = x$.

The GEO-SINR appears more closely described a pair of line segments with different slopes than a linear fit. Using linear regression, the coefficient of variation between the axes is merely $r^2 \simeq 0.031$, implying a low goodness-of-fit. Conversely, the MB-SINR model has a strong linear trend, with linear regression to the diagonal line incurring only 3.2% error and producing a large coefficient of variation $r^2 \simeq 0.968$ between the predicted and measured RSS. We conclude that the MB-SINR model is superior in capturing the additivity of interference than the canonical GEO-SINR.

D. Assessing the metricity parameter ζ

To facilitate algorithmic analysis of the GEO-SINR model, we introduced a metricity parameter ζ that reflects how well signal decay resembles a metric space, which we now evaluate.

Method and evaluation: Using values obtained for the RSS matrices in both testbeds, shown for TB-60 in Fig. 1a, we evaluate the minimal value of ζ, (as defined in Eqn. 2) for every directed node pair within communication range. As stated above, these experiments were performed with all motes using the same frequency at 2.44 GHz. The cumulative distribution function (CDF) of the resulting ζ values is shown in Fig. 4c, with the dashed lines representing the 2.44 GHz frequency. In both testbeds the values for ζ range from 1 to 10. However, note that the values in TB-60 are generally a bit larger than in TB-20. The increase is to be expected, since the challenging TB-60 environment both contains longer links with more variable signal strength as well as more variable signal attenuation due to obstacles.

Multiple frequencies: Attenuation models that consider (ground) reflection, like the two-ray model and multi-path fading ([13, Sec. 2]), suggest that on short distances, the reflecting signal can both cancel and amplify the main signal. Therefore, the attenuation of a signal over a short distance depends on the frequency. With that in mind, we performed additional experiments to obtain RSS matrices RSS^f for 8 different frequencies f ranging from 2.40 GHz to 2.48 GHz. We calculated ζ values separately for each RSS^f, and found that although they can vary significantly on a per link basis, the differences in the overall distributions were insignificant. The dashed lines in Fig. 4c are representative of other frequencies.

To factor out frequency-dependent fading, we computed for each node pair (s_v, r_v) the median $\widehat{\text{RSS}_v}$ of the eight RSS^f_v values (ranging over the different frequencies). We observe that ζ values of the matrix $\widehat{\text{RSS}}$ are significantly lower, as the thick lines in Fig. 4c indicate.

The frequency dependency is more apparent in TB-20, which suggests that signal reflection plays a relatively large role in that environment. The increased reliance on a particular frequency can be explained by the regular grid structure and condensed setting of TB-20 (Fig. 2), which makes the testbed a good candidate to observe (frequency dependent) multi-path fading phenomena. However, the links in TB-60 are on average longer and thus reflection plays a smaller role in signal attenuation. Furthermore, the greater number of obstacles in TB-60 may also explain the decreased dependency on frequency.

The observation that the channels have different fading properties brought us to introduce a new version of the LINK CAPACITY problem to incorporate different frequencies.

IV. PERFORMANCE GUARANTEES

We address the theoretical portion of our initial research question by showing that MB-SINR is amenable to algorithm design and analysis. We show that a large collection of analytic results carries over to the MB-SINR without change, as stated in the introduction. Namely, known results proved for general metric space do not depend on the particular value of the path loss constant α or that it is uniform. They merely apply the triangular inequality, for which Eqn. 2 applies equally well in arbitrary gain matrices.

We have shown in separate work [5] that it is computationally hard to approximate LINK CAPACITY within a factor of $2^{\zeta(1-o(1))}$ (see Appendix). That motivates examining the dependence of the approximation factor on ζ (or α). The previous results of [20], [29] can be seen to give $O(6^\zeta)$-approximations. We show in this section how to reduce that factor to $O(3^\zeta)$. Our proof also functions as an example, or "proof-of-concept", of how results are translated into MB-SINR with minor adjustments.

For LINK CAPACITY, approximation results carry over for the cases of: fixed power [20]; arbitrary power control [28], [29]; distributed setting based on regret minimization [2] and under jamming [8]; online setting [12], as well as the WEIGHTED version with linear power [21]. For SCHEDULING (a.k.a., *minimum length link scheduling*), results carry over for the cases of: linear power [10] and other fixed power [20]; arbitrary power control [28], [29]; distributed (multihop) setting [31], [19], [18]; stochastic dynamic setting [30]; and in the presence of Rayleigh fading [7]. Also assorted results on combinatorial spectrum auctions [25], [24], [18], and admission control (cognitive radio) [21]. Thus, an important

corollary of our definition is showing that much of the previous theoretical work in GEO-SINR is actually highly robust with respect to spatial signal variability.

Link capacity with multiple frequencies: Our observation in Section III-D that suggests that having a choice in the frequency to use results in smaller values of ζ, and thus better approximation factors, motivates us to generalize LINK CAPACITY. Namely, in MULTI-CHANNEL LINK CAPACITY, we assign links to a set of frequencies, but each link is only *eligible* to use a subset of the frequencies. As before, we want to assign as many links as possible with the constraint that those assigned to a given frequency form a feasible set.

This formulation considers links that experience significant frequency-dependent fading as not usable in that frequency. It does not take into consideration the possible decrease in *interference* due to such fading. One reason is that such fading is too unpredictable to expect any algorithm to utilize that to obtain better solutions than otherwise, and thus it is also not fair to compare with such a strong adversary. The other reason is that with arbitrary fading patterns, we are back in the *abstract SINR* model, for which very strong inapproximability results hold [14].

Additional definitions: To simplify notation we write $f_{uv} = f(s_u, r_v)$ and $f_v = f_{vv}$. We assume a total order $\prec$ on the links, where $\ell_v \prec \ell_w$ implies that $f_v \leq f_w$. We use the shorthand notation $\ell_v \prec L$ to denote that $\ell_v \prec \ell_u$ for all links ℓ_u in L. A power assignment P is *decay monotone* if $P_v \leq P_w$ whenever $\ell_v \prec \ell_w$, *reception monotone* if $\frac{P_w}{f_w} \leq \frac{P_v}{f_v}$ whenever $\ell_v \prec \ell_w$, and simply *monotone* if both properties hold. [1] This captures the main power strategies, including uniform and linear power.

We modify the notion of *affectance* [14], [22], [31]: The affectance $a_w^{\mathcal{P}}(v)$ of link ℓ_w on link ℓ_v under power assignment $\mathcal{P}$ is the interference of ℓ_w on ℓ_v normalized to the signal strength (power received) of ℓ_v, or

$$a_w(v) = \min\left(1, c_v \frac{P_w G_{wv}}{P_v G_{vv}}\right) = \min\left(1, \frac{P_w}{P_v}\frac{f_v}{f_{wv}}\right) \quad , \quad (3)$$

where $c_v = \frac{\beta}{1-\beta N/(P_v G_{vv})} > \beta$ is a constant depending only on universal constants and the signal strength G_{vv} of ℓ_v, indicating the extent to which the ambient noise affects the transmission. We drop $\mathcal{P}$ when clear from context. Furthermore let $a_v(v) = 0$. For a set S of links and link ℓ_v, let $a_v(S) = \sum_{\ell_w \in S} a_v(w)$ and $a_S(v) = \sum_{\ell_w \in S} a_w(v)$. Assuming S contains more than two links we can rewrite Eqn. 1 as $a_S(v) \leq 1$ and this is the form we will use. Observe that affectance is additive and thus $a_S(v) = a_{S_1}(v) + a_{S_2}(v)$ for any partition (S_1, S_2) of S.

We define a weight function $W_+(v, w) = a_v(w) + a_w(v)$, when $\ell_v \prec \ell_w$ and $W_+(v, w) = 0$, otherwise. The plus sign is to remind us that weights are from smaller to larger decay links. Also, $W_+(X, v) = \sum_{\ell_w \in X} W_+(w, v)$, representing the sum of the in- and out-affectances (as in Eqn. 3) of a link v to and from those links in set X that have smaller decay.

[1] This corresponds to *length monotone* and *sublinear* power assignments in GEO-SINR.

A set S of links is *anti-feasible* if $a_v(S) \leq 2$ for every link $\ell_v \in S$ and *bi-feasible* if both feasible and anti-feasible [19]. More generally, for $K \geq 1$, S is K*-feasible* (K*-anti-feasible*) if $a_v(S) \leq 1/K$ ($a_S(v) \leq 2/K$), and K*-bi-feasible* if both.

Approximation of MULTI-CHANNEL LINK CAPACITY: Given a set L of links using monotone power, the classic LINK CAPACITY problem is to find a maximum subset $S \subseteq L$ of links that can successfully transmit simultaneously. We modify the LINK CAPACITY problem to fit our observations on the use of multiple frequencies:

MULTI-CHANNEL LINK CAPACITY

Given: A set L of n links using monotone power, and k subsets k subsets $L_1, L_2, \ldots, L_k \subseteq L$.

Find: Sets $S_1, S_2, \ldots, S_k$ with $S_i \subseteq L_i$ and S_i feasible, for $i = 1, 2, \ldots, k$.

Maximize: $|S_1 \cup S_2, \ldots \cup S_k|$.

Here L_i represents the links that are eligible for frequency i and S_i those scheduled for that frequency.

We extend a greedy algorithm for LINK CAPACITY [20] and show that it gives equally good approximation for MULTI-CHANNEL LINK CAPACITY, even in MB-SINR.

Algorithm 1 MULTI-CHANNEL LINK CAPACITY in MB-SINR

Let L be a set of links using monotone power $\mathcal{P}$ and $L_1, L_2, \ldots, L_k \subseteq L$ be subsets.
Set $X_1, X_2, \ldots X_k \leftarrow \emptyset$
for $\ell_v \in L$ in order of increasing f_v values **do**
  for $i \leftarrow 1 \ldots k$ **do**
    if $W_+(X_i, v) \leq 1/2$ **then**
      $X_i \leftarrow X_i \cup \{\ell_v\}$
      break
for each X_i **do**
  $S_i \leftarrow \{\ell_v \in X_i | \sum_{\ell_w \in X_i} a_w(v) \leq 1\}$
return $(S_1, S_2, \ldots, S_k)$

Note that the sets returned by Algorithm 1 are feasible by construction.

We turn to proving a performance guarantee for the algorithm. The following key result bounds the affectance of a feasible set to a (shorter) link outside the set to a constant. A similar but weaker bound was first introduced by Kesselheim and Vöcking [31].

Theorem 1. *Let L be a $3^\zeta/\beta$-bi-feasible set with monotone power assignment $\mathcal{P}$ and let ℓ_v be a link (not necessarily in L) with $\ell_v \prec L$. Then, $W_+(v, L) = O(1)$.*

We prove Theorem 1 by splitting it into two lemmas bounding in-affectance for links in a feasible set and similarly bounding out-affectance for links in an anti-feasible set.

Lemma 2. *Let L be a $3^\zeta/\beta$-feasible set with monotone power assignment $\mathcal{P}$ and ℓ_v be any link with $\ell_v \prec L$. Then, $a_L^{\mathcal{P}}(v) = O(1)$.*

Proof: The basic idea is to identify a "proxy" for ℓ_v within the set L. Namely, we bound the affectance of L on ℓ_v in terms of the affectance on the "nearest" link ℓ_u in L, which is small since L is feasible and contains ℓ_u.

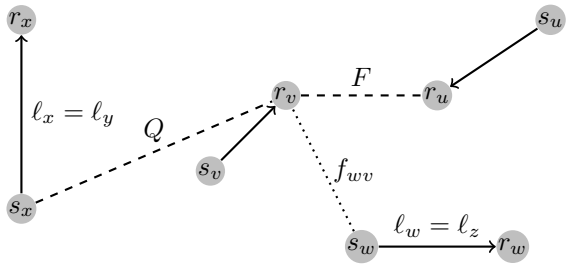

Fig. 6: We show that for each link ℓ_x it holds that $Q \geq \frac{F}{2^\zeta}$.

Formally, consider the link $\ell_u = (s_u, r_u) \in L$ such that $F := f(r_v, r_u)$ is minimum and link $\ell_w = (s_w, r_w) \in S$ such that $f_{wv} = f(s_w, r_v)$ is minimum (possibly $\ell_u = \ell_w$). Let ℓ_x be an arbitrary link in L and define $Q = f_{xv}$. See Fig. 6.

We first show that

$$F \leq 2^\zeta Q \ . \tag{4}$$

Let ℓ_y, ℓ_z be renamings of the links ℓ_x, ℓ_w such that $f_y = \max(f_x, f_w)$ and $f_z = \min(f_x, f_w)$.

By definition of ℓ_u and ℓ_w, it holds that $\max(f_{yv}, f_{zv}) \leq Q$. Thus, using the weak triangular inequality,

$$f(s_y, s_z)^{1/\zeta} \leq f_{yv}^{1/\zeta} + f_{zv}^{1/\zeta} \leq 2Q^{1/\zeta} \ . \tag{5}$$

Using Eqn. 5 and that $f_z \leq f_y$, it holds that

$$f_{yz}^{1/\zeta} \leq f_z^{1/\zeta} + f(s_y, s_z)^{1/\zeta} \leq f_y^{1/\zeta} + 2Q^{1/\zeta} \ . \tag{6}$$

By the feasibility condition on L, $a_y(z) \leq \beta/3^\zeta$, while by definition of affectance and reception monotonicity (i.e., $P_y/f_y \leq P_z/f_z$),

$$a_y(z) = c_z \frac{P_y}{P_z} \frac{f_z}{f_{yz}} \geq \beta \frac{f_y}{f_{yz}} \ .$$

Combining the two bounds on $a_y(z)$, we get that $3^\zeta \cdot f_y \leq f_{yz}$. That, combined with Eqn. 6 and canceling a f_y factor, gives that $3^\zeta \leq \left(1 + 2(Q/f_y)^{1/\zeta}\right)^\zeta$, which implies that $f_y \leq Q$ and further that $f_w \leq f_y \leq Q$. Then, by the definitions of F, ℓ_w and Q,

$$F^{1/\zeta} = f(r_v, r_w)^{1/\zeta} \leq f_{wv}^{1/\zeta} + f_w^{1/\zeta} \leq 2 \cdot Q^{1/\zeta} \ , \tag{7}$$

implying Eqn. 4, as desired.

Now, using the weak triangular inequality, $F \leq \min(f(r_y, r_v), f(r_z, r_v))$ and Eqn. 7, we get that

$$\begin{aligned} f_{xu}^{1/\zeta} &\leq f_{xv}^{1/\zeta} + f(r_v, r_u)^{1/\zeta} \leq Q^{1/\zeta} + F^{1/\zeta} \\ &\leq Q^{1/\zeta} + 2Q^{1/\zeta} = 3^\zeta Q = 3^\zeta f_{xv} \ . \end{aligned} \tag{8}$$

Observe that since $f_v \leq f_u$ and power is monotone, it holds that $c_v \leq c_u$. Then, using Eqn. 8 and the definition of affectance,

$$a_x(v) = c_v \frac{P_x}{f_{xv}} \frac{f_v}{P_v} \leq c_u \frac{3^\zeta P_x}{f_{xu}} \frac{f_u}{P_u} = 3^\zeta a_x(u) \ .$$

Finally, letting $L_w = L \setminus \{\ell_w\}$, we sum over all links in L,

$$a_L(v) = a_w(v) + a_{L_w}(v) \leq 1 + 3^\zeta a_{L_w}(u) \leq 1 + 3^\zeta \cdot \frac{\beta}{3^\zeta} = O(1) \ ,$$

using the feasibility assumption for the last inequality. ∎

For anti-feasible sets a similar result can be shown, with an essentially identical (omitted) proof, swapping the roles of senders and receivers of the links.

Lemma 3. *Let L be a $3^\zeta/\beta$-anti-feasible set with monotone power assignment $\mathcal{P}$ and let ℓ_v be a link with $\ell_v \prec L$. Then, $a_v^{\mathcal{P}}(L) = O(1)$.*

Combining Lemma 2 and 3 implies Theorem 1.

Finally, to show that Algorithm 1 yields an approximation of factor $O(3^\zeta)$ we will use an adaptation of the following signal-strengthening lemma from [9, Prop. 8] and a lemma generalizing a popular argument used to show that the size of a subset of links of another set of links is large.

Lemma 4 ([9])**.** *Let L be a feasible set and $K \geq 1$ be a value. Then, there exists a K-bi-feasible subset of L of size $\Omega(|L|/K)$.*

Proving $O(3^\zeta)$ approximation for Algorithm 1 is now straightforward.

Theorem 5. *Algorithm 1 yields a $O(3^\zeta)$ approximation for* MULTI-CHANNEL LINK CAPACITY.

Proof: Let L be a set of links and let $L_1, L_2, \ldots, L_k \subseteq L$ be subsets of L where L_i contains the links that are eligible in frequency i. Let $OPT = OPT_1 \cup OPT_2 \cup \ldots \cup OPT_k$ be an optimum solution to MULTI-CHANNEL LINK CAPACITY on L. Let $K = 3^\zeta/\beta$. By Lemma 4, there is a K-bi-feasible subset OPT_i' in OPT_i of size $\Omega(|OPT_i|/K)$, for each $i \in \{1, \ldots, k\}$. Let $OPT' = OPT_1' \cup OPT_2' \cup \ldots \cup OPT_k'$.

Let $S = S_1 \cup S_2 \cup \ldots S_k$ and $X = X_1 \cup X_2 \cup \ldots X_k$ be the sets computed by Algorithm 1 on input L. We first bound $|S|$ in terms of $|X|$ and then $|X|$ in terms of $|OPT'|$. To bound $|S|$ to $|X|$ we bound $|S_i|$ to $|X_i|$ for every $i \in \{1 \ldots k\}$. Note that by the construction of X_i, $a_{X_i}(X_i) = W_+(X_i, X_i) \leq |X_i|/2$, and thus the average in-affectance of links in X_i is at most $1/2$. Since each S_i consists of the links in X_i of affectance at most $1/2$, by Markov's inequality, $|S_i| \geq |X_i|/2$.

By the definition of the algorithm, $W_+(X_i, \ell_w) > 1/2$, $\forall \ell_w \in OPT' \setminus X, X_i \in X$. Summing over all links ℓ_w in $OPT' \setminus X$, we get that $W_+(X_i, OPT' \setminus X) > |OPT' \setminus X|/2$. Furthermore, since OPT' contains k K-feasible sets, it follows by Theorem 1 that $W_+(\ell_v, OPT') = O(k)$, for each $\ell_v \in X$. Summing over all links in X_i, we get that $W_+(X_i, OPT) = O(k|X_i|)$. Combining yields that for any set X_i we have $|OPT' \setminus X|/2 < W_+(X_i, OPT' \setminus X_i) \in O(k|X_i|)$, giving that $|X_i| = \Omega(|OPT' \setminus X|/k)$.

Summing over i then gives $|X| = \sum_i |X_i| = \Omega(|OPT' \setminus X|)$. Thus, the solution output by the algorithm satisfies $|S| \geq |X|/2 = \Omega(|OPT'|) = \Omega(|OPT|/K) = \Omega(|OPT|/3^\zeta)$. ∎

In summary, the metricity definition implies that a large range of algorithmic results from GEO-SINR carries over without change. Thus, MB-SINR has both the desired generality and amenability to algorithmic analysis. We also extend known

results on LINK CAPACITY to handle frequency-sensitive links, and improve the dependence of the approximation on ζ along the way.

V. RELATED WORK

Numerous experimental results have indicated that simplistic range-based models of wireless reception are insufficient [11], [47], [33], [1], [39], [48], [46]. Besides directionality and asymmetry, signal strength is not well predicted by distance. Interference patterns are also insufficiently explained by pairwise relationships, suggesting the need for additive interference models, both experimentally [33], [37], [34] and analytically [37], [36], [27].

The weakness of the known prescriptive models for interference and packet reception has led experimentalists to form models based on measurements. Son, Krishnamachari and Heidemann [44] showed that the SINR formula, using separately measured RSS values, is the main factor in predicting PRR. They found PRR to be dependent on the number of interferers, which was not supported in later studies [34], [6] and attributed to hardware variability or the quality of the CC1000 radios used. Reis et al. [42] independently proposed a similar approach on a 802.11 platform. They found substantial variability across nodes, and that similarity across time was sufficient over moderate time scales of minutes to hours, but that prediction accuracy degrades over longer periods.

Maheshwari, Jain and Das [34] compared different models of interference using two testbeds with variations in hardware, power level, and indoor/outdoor. They concluded that the physical model gives best accuracy, albeit less than perfect. In their followup workshop paper [35], they focus on the relationship of *joint interference* (SINR with multiple interferers) to PRR. They gave strong evidence that the basic formula works, and verify the *additivity* of the SINR model.

Chen and Terzis [6] proposed a method for calibrating RSSI readings to combine interference measurements from different motes. They found that Tmote Sky motes consistently report RSSI values inaccurately, even reporting non-injective relationships. By aligning measurements from different motes, they obtained much better SINR vs. PRR relationship, reducing the width of the intermediate range significantly. They suggested that this may explain much of the imperfect relationship observed in [34].

Measurement-based approaches have also been proposed in the context of 802.11 [16], [41], [43], where carrier sense and control packets complicate the picture. Recent efforts have focused on reducing the required measurements by deducing interference using, e.g., linear algebra [40] or regression [26]. Boano et al. [4] also studied the impact of external interference on sensor-network MAC protocols, and identified mechanisms to improve their robustness.

The engineering literature has introduced various extensions in order to capture reality more faithfully. In the *two-ray* model [13], which captures reflection off the ground, signal decays in the near-term as a certain polynomial, but as a higher degree polynomial further away. More generally, the *multi-ray* model has the signal (in dBm, log scale) decaying via a piecewise linear model with segments of increasing slopes. The function is typically empirically determined. We note that these models can be captured by MB-SINR, with ζ as the steepest slope.

There are also *empirical models* [13], such as the *Okumura* and *Hata* models, that take the environment into account. These could also be used to generate a gain matrix. Also, accurate estimates can be obtained via general *ray tracing* when highly detailed information is available.

Some studies have allowed signal strength to fluctuate from the geometric path loss by up to a constant factor [38], [22]. This is of limited help in general, however, since even minor fluctuations of the value of α can cause arbitrarily large changes in signal strength [15].

Various probabilistic models also exist. On one hand, they are means to prescribe non-geometric components to signal reception, which is useful for simulation studies (which MB-SINR cannot provide), but which could be captured more accurately by actual measurements. On the other hand, these can also model aspects that are necessarily random, in which case they could complement the deterministic MB-SINR.

VI. CONCLUSION

Tackling the proliferation of wireless technologies requires a shared understanding of interference from theoretical and experimental vantage points. Yet a raft exists between the research communities since analytical models are not realistic in practice, and practical models are too complex for analysis. We seek to bridge this gap in this paper.

We generalize the simple geometric SINR model of wireless interference (GEO-SINR) — the cornerstone of recent advances in algorithmic theory for ad-hoc wireless networks — with an additional metricity parameter ζ that describes an environment's deviation from a metric space. The parameter enables received signal strength (RSS) to be used in place of geometric predictions of signal decay in SINR without compromising the analytic power of the model. In terms of generality, the concept of ζ allows any natural SINR-type algorithm that works in metric space to be equally applicable in MB-SINR.

We ran experiments to assess the predictive power of our measurement based SINR model (MB-SINR) compared to GEO-SINR, finding that MB-SINR has significantly more power than GEO-SINR at predicting the success of a given communication link. The evaluation was conducted on a small homogeneous test environment (TB-20) as well as a larger, complex environment (TB-60) that included significant mote clustering, signal reflection, and limited line-of-sight.

Finally, we demonstrated how theoretical results from the literature on algorithmic GEO-SINR carry over to our model with minimal effort, generalizing a constant-approximation algorithm for LINK CAPACITY to a multiple-channel version in the MB-SINR as an example. In addition to showing that the MB-SINR model is a powerful tool for predicting wireless performance in real environments compared to the canonical physical models, our approach illustrates a methodology for harmonizing algorithmic theory of wireless interference with real-world observations.

REFERENCES

[1] D. Aguayo, J. Bicket, S. Biswas, G. Judd, and R. Morris. Link-level measurements from an 802.11b mesh network. *ACM SIGCOMM Computer Communication Review*, 34(4):121–132, 2004.

[2] E. Ásgeirsson and P. Mitra. On a game theoretic approach to capacity maximization in wireless networks. In *INFOCOM*, 2011.

[3] N. Baccour, A. Koubaa, L. Mottola, M. A. Zuniga, H. Youssef, C. A. Boano, and M. Alves. Radio link quality estimation in wireless sensor networks: a survey. *ACM Trans. Sensor Networks (TOSN)*, 8(4):34, 2012.

[4] C. A. Boano, T. Voigt, N. Tsiftes, L. Mottola, K. Römer, and M. A. Zúniga. Making sensornet MAC protocols robust against interference. In *Wireless Sensor Networks*, pages 272–288. Springer, 2010.

[5] M. H. L. Bodlaender and M. M. Halldórsson. Beyond basic SINR: Modeling spatial variability in wireless networks. Manuscript, Nov. 2013.

[6] Y. Chen and A. Terzis. On the mechanisms and effects of calibrating RSSI measurements for 802.15.4 radios. In *Wireless Sensor Networks*, pages 256–271. Springer, 2010.

[7] J. Dams, M. Hoefer, and T. Kesselheim. Scheduling in wireless networks with Rayleigh-fading interference. In *SPAA*, pages 327–335, 2012.

[8] J. Dams, M. Hoefer, and T. Kesselheim. Jamming-resistant learning in wireless networks. *arXiv preprint arXiv:1307.5290*, 2013.

[9] A. Fanghänel, T. Kesselheim, H. Räcke, and B. Vöcking. Oblivious interference scheduling. In *PODC*, pages 220–229, August 2009.

[10] A. Fanghänel, T. Kesselheim, and B. Vöcking. Improved algorithms for latency minimization in wireless networks. In *ICALP*, pages 447–458, July 2009.

[11] D. Ganesan, B. Krishnamachari, A. Woo, D. Culler, D. Estrin, and S. Wicker. Complex behavior at scale: An experimental study of low-power wireless sensor networks. Technical report, UCLA/CSD-TR 02, 2002.

[12] O. Göbel, M. Hoefer, T. Kesselheim, T. Schleiden, and B. Vöcking. Online independent set beyond the worst-case: Secretaries, prophets, and periods. *CoRR*, abs/1307.3192, 2013.

[13] A. Goldsmith. *Wireless Communications*. Cambridge Univ. Press, 2005.

[14] O. Goussevskaia, M. M. Halldórsson, R. Wattenhofer, and E. Welzl. Capacity of Arbitrary Wireless Networks. In *INFOCOM*, pages 1872–1880, April 2009.

[15] Z. Gu, G. Wang, and Y. Wang. Path-loss fluctuations towards robust scheduling algorithms in the SINR model. In *MASS*, pages 416–424. IEEE, 2012.

[16] R. Gummadi, D. Wetherall, B. Greenstein, and S. Seshan. Understanding and mitigating the impact of RF interference on 802.11 networks. In *SIGCOMM*, pages 385–396. ACM, 2007.

[17] P. Gupta and P. R. Kumar. The Capacity of Wireless Networks. *IEEE Trans. Information Theory*, 46(2):388–404, 2000.

[18] M. M. Halldórsson, S. Holzer, P. Mitra, and R. Wattenhofer. The power of non-uniform wireless power. In *SODA*, 2013.

[19] M. M. Halldórsson and P. Mitra. Nearly optimal bounds for distributed wireless scheduling in the SINR model. In *ICALP*, 2011.

[20] M. M. Halldórsson and P. Mitra. Wireless Capacity with Oblivious Power in General Metrics. In *SODA*, 2011.

[21] M. M. Halldórsson and P. Mitra. Wireless capacity and admission control in cognitive radio. In *INFOCOM*, pages 855–863, 2012.

[22] M. M. Halldórsson and R. Wattenhofer. Wireless Communication is in APX. In *ICALP*, 2009.

[23] J. Håstad. Clique is hard to approximate within $n^{1-\epsilon}$. *Acta Mathematica*, 182:105–142, 1999.

[24] M. Hoefer and T. Kesselheim. Secondary spectrum auctions for symmetric and submodular bidders. In *EC*, pages 657–671, 2012.

[25] M. Hoefer, T. Kesselheim, and B. Vöcking. Approximation algorithms for secondary spectrum auctions. In *SPAA*, 2011.

[26] J. Huang, S. Liu, G. Xing, H. Zhang, J. Wang, and L. Huang. Accuracy-aware interference modeling and measurement in wireless sensor networks. In *ICDCS*, pages 172–181. IEEE, 2011.

[27] A. Iyer, C. Rosenberg, and A. Karnik. What is the right model for wireless channel interference? *IEEE Transactions on Wireless Communications*, 8(5):2662–2671, 2009.

[28] T. Kesselheim. A Constant-Factor Approximation for Wireless Capacity Maximization with Power Control in the SINR Model. In *SODA*, 2011.

[29] T. Kesselheim. Approximation algorithms for wireless link scheduling with flexible data rates. In *ESA*, pages 659–670, 2012.

[30] T. Kesselheim. Dynamic packet scheduling in wireless networks. In *PODC*, pages 281–290, 2012.

[31] T. Kesselheim and B. Vöcking. Distributed contention resolution in wireless networks. In *DISC*, pages 163–178, August 2010.

[32] S. Khot and A. K. Ponnuswami. Better inapproximability results for maxclique, chromatic number and min-3lin-deletion. In *Automata, Languages and Programming*, pages 226–237. Springer, 2006.

[33] D. Kotz, C. Newport, R. S. Gray, J. Liu, Y. Yuan, and C. Elliott. Experimental evaluation of wireless simulation assumptions. In *MSWiM*, pages 78–82. ACM, 2004.

[34] R. Maheshwari, S. Jain, and S. R. Das. A measurement study of interference modeling and scheduling in low-power wireless networks. In *SenSys*, pages 141–154, 2008.

[35] R. Maheshwari, S. Jain, and S. R. Das. On estimating joint interference for concurrent packet transmissions in low power wireless networks. In *WinTech*, pages 89–94. ACM, 2008.

[36] T. Moscibroda and R. Wattenhofer. The Complexity of Connectivity in Wireless Networks. In *INFOCOM*, 2006.

[37] T. Moscibroda, R. Wattenhofer, and Y. Weber. Protocol Design Beyond Graph-Based Models. In *Hotnets*, November 2006.

[38] T. Moscibroda, R. Wattenhofer, and A. Zollinger. Topology control meets SINR: The scheduling complexity of arbitrary topologies. In *MOBIHOC*, pages 310–321, 2006.

[39] J. Padhye, S. Agarwal, V. N. Padmanabhan, L. Qiu, A. Rao, and B. Zill. Estimation of link interference in static multi-hop wireless networks. In *IMC*, 2005.

[40] X. Qi, Y. Wang, Y. Wang, L. Xu, and C. Hu. EIM: Efficient online interference measurement in wireless sensor networks. In *WiOpt*, pages 548–555. IEEE, 2013.

[41] L. Qiu, Y. Zhang, F. Wang, M. K. Han, and R. Mahajan. A general model of wireless interference. In *MobiCom*, pages 171–182, 2007.

[42] C. Reis, R. Mahajan, M. Rodrig, D. Wetherall, and J. Zahorjan. Measurement-based models of delivery and interference in static wireless networks. In *SIGCOMM*, pages 51–62, 2006.

[43] V. Sevani and B. Raman. SIR based interference modeling for wireless mesh networks: A detailed measurement study. In *COMSNETS*, pages 1–10. IEEE, 2012.

[44] D. Son, B. Krishnamachari, and J. Heidemann. Experimental study of concurrent transmission in wireless sensor networks. In *SenSys*, pages 237–250. ACM, 2006.

[45] TI Corporation. CC2510Fx/CC2511Fx: Low-power SoC (system-on-chip) with MCU, memory, 2.4 GHz RF transceiver, and USB controller. http://www.ti.com/product/cc2511f32. [Online; accessed 27-Nov-2013].

[46] M. Z. Zamalloa and B. Krishnamachari. An analysis of unreliability and asymmetry in low-power wireless links. *ACM Transactions on Sensor Networks (TOSN)*, 3(2):7, 2007.

[47] J. Zhao and R. Govindan. Understanding packet delivery performance in dense wireless sensor networks. In *SenSys*, pages 1–13. ACM, 2003.

[48] G. Zhou, T. He, S. Krishnamurthy, and J. A. Stankovic. Models and solutions for radio irregularity in wireless sensor networks. *ACM Transactions on Sensor Networks (TOSN)*, 2(2):221–262, 2006.

APPENDIX

We present here a hardness result for the approximation of LINK CAPACITY, taken from [5]. It shows that approximation factors must necessarily be exponential in ζ.

A power assignment is *oblivious* if it the power assigned to a link ℓ_v depends only on the fading on the link (but not its relationship to other links).

Theorem 6. *Oblivious power* LINK CAPACITY *with variable signal decay is hard to approximate within* $2^{\zeta(1-o(1))}$*-factor.*

Proof: By reduction from the maximum independent set problem in graphs. Given graph $G(V, E)$, form a link $\ell_i = (s_i, r_i)$ for each vertex $v_i \in V$. Let α be arbitrary. The fading matrix is given by:

$$f_{ij} = f(s_i, r_j) = \begin{cases} n^\alpha & \text{if } i = j \\ n^\alpha/2 & \text{if } v_i v_j \in E \\ n^{\alpha+1} & \text{if } v_i v_j \notin E. \end{cases}$$

Since all links are of the same decay, any oblivious power assignment will be uniform. We then observe that $P/f_i = P/n^\alpha$ and

$$a_i(j) = \frac{P/f_{ij}}{P/f_j} = \frac{n^\alpha}{f_{ij}} = \begin{cases} 2 & \text{if } v_i v_j \in E \\ 1/n & \text{if } v_i v_j \notin E. \end{cases}$$

Hence, a set $S \subseteq L$ of links is feasible iff $V_S = \{v_i \in V : \ell_i \in S\}$ is an independent set in G. Thus, the $\Omega(n^{1-o(1)})$-computational hardness of MAX INDEPENDENT SET [32] implies equivalent hardness for LINK CAPACITY.

Regarding metricity, let us define $f(s_i, s_j) = f(r_i, r_j) = n^\alpha$. Then we can verify that for any triple a, b, c of points used in L, $f_{ac} \leq n^{\alpha+1}$ while $f_{ab}, f_{bc} \geq n^\alpha$. So, for $\zeta = \log n$, $f_{ac}^{1/\zeta} \leq 2^{\alpha+1}$, while $f_{ab}^{1/\zeta} + f_{bc}^{1/\zeta} = 2^\alpha + 2^\alpha = 2^{\alpha+1}$. Thus, $\zeta \leq \log n$. The hardness gap in terms of ζ is then $\Omega(2^{\zeta(1-o(1))})$. ∎